Viscoelastoplastic cyclic behaviour of sail materials

Wassim Dib, Ali Tourabi, Guilhem Blès

VISCOELATOPLASTIC CYCLIC BEHAVIOUR OF SAIL MATERIALS

W. Dib, University of Grenoble, France.
A. Tourabi, University of Grenoble, France.
G. Bles, Engineering School ENSIETA/University of Brest/ENIB - Laboratory LBMS, France.

SUMMARY

A tensorial visco-elasto-hysteresis model has been used previously in order to describe the thermomechanical behaviour of woven fabrics [1, 2]. Thus, it takes into account the essential features of behaviour, such as the steady state viscous stress as a function of strain and strain rate, the time-independent irreversible behaviour and the instantaneous modulus increasing with the strain. The aim of the study is to suggest the interest of the theory in the field of sail fabrics concerning characterization, testing and design. Moreover, we focus attention on two questions which are of fundamental interest, both at the level of principles and in the field of technological research, namely the viscous behaviour of sail fabrics and his nonlinear character.

~~~~~~
~~~~~~

NOMENCLATURE

m_s	Surface density (g m^{-2})
ρ_0	Density in the initial configuration (kg m^{-3})
ρ_t	Density in the current configuration (kg m^{-3})
σ	Cauchy stress for uniaxial tension (Pa)
Σ	Piola-Kirchhoff-1 stress (Pa)
σ_m	Specific stress (J/kg)
ε_l	Logarithmic strain for uniaxial tension (%)
D	Strain rate for uniaxial tension (s^{-1})

1. INTRODUCTION

Some authors study the woven fabrics at the mesoscopic scale of the weave and proposed nonlinear elastic constitutive laws [5]. We consider the fabric as a continuum, at the macroscopic scale, in order to propose anisotropic highly nonlinear visco-elasto-plastic constitutive laws. Often, the structural modelling of sails considers isotropic [9] or anisotropic linear elastic constitutive laws [7, 11, 15]. Paton et al. [10] observed that an accurate modelling of racing yacht sails demands an accurate structural modelling including a precise constitutive law for the material. We aim to study the nonlinear viscosity and nonlinear elasticity of sail fabrics in order to propose more accurate constitutive models.

A tensorial visco-elasto-hysteresis model has been used previously in order to describe the thermomechanical behaviour of woven fabrics [1, 2]. The aim of the present study was to discern and to characterize some generic aspects of the behaviour of sail fabrics, starting with the stress-strain-time experimental measurements. Two materials were studied, branded “Dacron 300 SF HTM” and “Dacron 300 SF HTP plus”. Monotonous and cyclic tensile loadings with creep and relaxation periods were carried out at constant strain and stress rates. The results were examined and analysed to characterize the behaviour in the warp and fill directions. In addition, we focused attention on the viscous behaviour of these two materials. This experimental study was completed by an implementation of the proposed theoretical approach in the simple linear viscoelastic case. In order to characterize the impact of viscous effects on the structural behaviour of sails, a structural analysis of a flat sail is proposed using finite element method.

Section 2 gives an overview of the theoretical approach. The materials, the sample and the assumptions about experimental data will be introduced in section 3. The analysis and interpretation of experimental results are presented in section 4. Finally, section 5 will be devoted to implementation of the model and to structural analysis.

2. OVERVIEW OF THE THEORETICAL APPROACH

A phenomenological approach at the macroscopic level is adopted in order to predict the cyclic thermomechanical behaviour of woven materials [1, 4]. This approach is based on a fundamental superimposition assumption, which considers the stress applied $\sigma(\varepsilon,\dot{\varepsilon},\xi)$ like a sum of three stress components:

$$\sigma(\varepsilon,\dot{\varepsilon},\xi)=\sigma_{\mathrm{V}}(\varepsilon,\dot{\varepsilon})+\sigma_{\mathrm{r}}(\varepsilon)+\sigma_{\mathrm{h}}(\varepsilon,\xi) \qquad \textbf{(1)}$$

The stress component $\sigma_{\mathrm{h}}(\varepsilon,\xi)$ is elastoplastic and always irreversible; it is a function of the current strain ε and of its history denoted here by the parameter ξ. The stress component $\sigma_{\mathrm{r}}(\varepsilon)$ is nonlinear elastic. The stress component $\sigma_{\mathrm{V}}(\varepsilon,\dot{\varepsilon})$ is viscoelastic with a nonlinear viscosity as this stress has a nonlinear relation with the strain rate $\dot{\varepsilon}$ and is also a function of the strain ε. The Figure 1-a illustrates this assumption, proposing a visco-elasto-hysteresis model in the one-dimensional case. Each stress component is presented by a symbolic model. Its mechanical behaviour is qualitatively illustrated in Figure 1-b to 1-e.

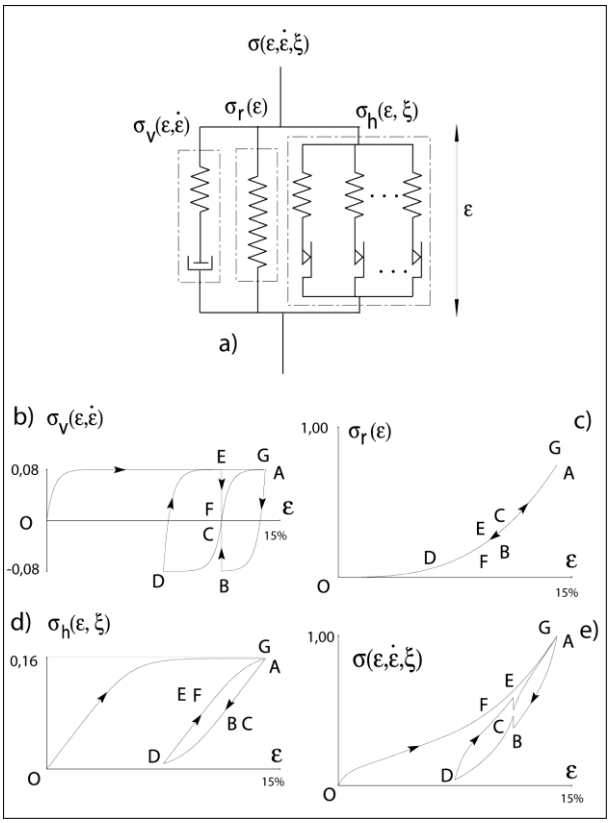

Figure 1: Visco-elasto-hysteresis model

The figure 1-e illustrates the effect of the stress component $\sigma_h(\varepsilon,\xi)$, which makes the C and F points different at the end of BC and EF relaxation periods. In the case of viscoelastic behaviour, these ends of relaxation periods are coincident (Fig. 1-b).

3. EXPERIMENTAL TECHNIQUES

Two sail fabrics were studied, branded "Dacron 300 SF HTM" and "Dacron 300 SF HTP plus". These materials are woven with polyester fibers. Their mass densities are respectively m_s= 312 gm^{-2} and m_s= 298 gm^{-2}.

The sample is clamped to the testing machine by a pair of swivel jaws, able to perform off-axis tensile tests. In the current study, tests were conducted in the warp and fill directions.

The length of the sample is L=300mm and the width is w=50mm. The sample axial strain ε_{loc} is measured locally by an optical system, with the help of CCD camera. This measurement method, with no contact, is especially adapted for woven materials. Black marks or targets are pre-printed on the specimen. The optical system tracks the targets and trajectories are recorded, during the test (Fig.2). The measurement base B is equal to 100mm, and the local strain is obtained by the relative displacement Δz_{loc} of the targets:

$$\varepsilon_{loc} = \frac{\Delta z_{loc}}{B}$$

A global axial strain measurement ε_{glo} is also obtained, by the relative displacement Δz_{glo} of the two samples edges. The global strain ε_{glo} takes into account the deformation of the whole sample, including the two clamping zones. Thus, we introduce a notion of equivalent length L_{equ} of the sample (L_{equ}>L), such as:

$$\varepsilon_{glo} = \frac{\Delta z_{glo}}{L_{equ}} \quad and \quad \varepsilon_{glo} = \varepsilon_{loc}$$

Consequently, the equivalent length L_{equ} is determined by equating the two strain measurements. The mean value and standard deviation of equivalent length are indicated with the confidence interval (c.i.) of 95%:

$$L_{equ} = 329 \pm 1\text{mm (95\% c.i., n = 10)}$$

In the following we will not distinguish between local and global strain. The sample axial strain will be denoted by ε, such as:

$$\varepsilon = \varepsilon_{glo} = \varepsilon_{loc}$$

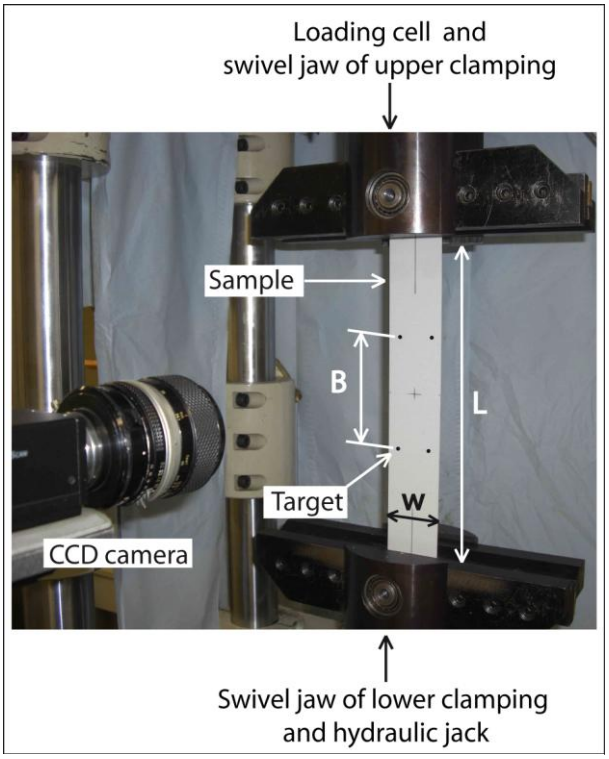

Figure 2 - Sample attached to hydraulic testing machine

In order to extend this definition to the case of large deformation, we introduce the stretch λ, such as:

$$\lambda = 1 + \varepsilon$$

and the logarithmic strain, such as:

$$\varepsilon_l = \ln(\lambda) = \varepsilon - \frac{1}{2}\varepsilon^2 + O(\varepsilon^2) \qquad \textbf{(2)}$$

The logarithmic strain rate corresponds to the axial strain-rate D, such as:

$$D = \dot{\varepsilon}_l = \frac{\dot{\lambda}}{\lambda}$$

During a tensile test at a given constant strain-rate D_0, the displacement speed of the sample edges, is controlled, as:

$$\dot{\Delta} z_{glo}(t) = L_{equ}\ (e^{D_0 t} - 1)$$

where t denotes the time.

The stress applied to the sample was calculated from the load measure according to the assumptions of continuum mechanics. The material is assumed to be a homogeneous continuum. The tensile stress was calculated as the specific stress σ_m, especially useful in the case of woven materials, such as:

$$\sigma_m = \frac{\sigma}{\rho_t} \quad \text{and} \quad \sigma_m = \frac{\Sigma}{\rho_0} \qquad \textbf{(3)}$$

where σ and Σ are the Cauchy and Piola-Kirchhoff-1 stresses; ρ_t and ρ_0 the densities in the current and initial configurations. At first, this definition of stress may be surprising because it's expressed as $N.m.kg^{-1}$ or $J.kg^{-1}$. Besides its theoretical interest, this definition does not require the thickness measurement of the sample, which is a very delicate operation. Indeed, if we consider the surface density m_s of the material and the initial cross-section S of the sample, we obtain:

$$\sigma_m = \frac{F}{S\,\rho_0} = \frac{F}{w m_s} \qquad \textbf{(4)}$$

the specific stress σ_m derives from the ratio F/w of the force per unit length.

4. PRESENTATION AND ANALYSIS OF EXPERIMENTAL RESULTS

4.1 MONOTONOUS AND CYCLIC TENSILE TESTS AT CONSTANT STRESS RATE

Two cyclic tensile tests interrupted by creep periods were conducted on the "Dacron 300 SF HTP plus". In the following, these tests will be called test 1 and test 2. The stress rate was controlled and maintained constant at $\dot{\sigma}_m = 671\ J/(kg.s)$. The loading and unloading processes were broken by some creep periods, during which the stress is constant. The duration of each period has been set at one hour. The results of the two tests are given in figure 3. Test 2 presents one loading–unloading cycle (cycle $0c_2h_2m_2$). Test 1 was controlled at the same stress rate as test 2, but presents no cycle, it is a monotonous tensile broken with creep periods (loading 0e1).

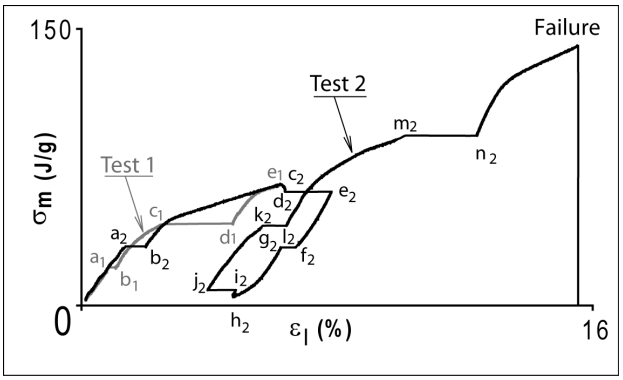

Figure 3 - Results of monotonous and cyclic tensile tests with creep periods ($\dot{\sigma}_m = 671\ J/(kg.s)$)

During the creep stages, the strain may decrease (f_2g_2) or increase (k_2l_2) according to the location of the creep sequence in the stress–strain hysteresis loop. If the creep stage breaks a first or monotonous loading, the strain always increases regardless of creep location (Fig.4).

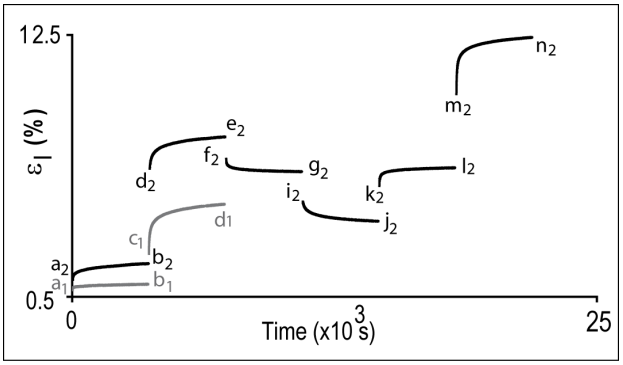

Figure 4 - Strain versus time during creep periods

Test 2 (Fig. 3) shows that the creep strain amplitude could be null, if the creep stage breaks the loading branch at a special point. Indeed, the sign of variation of strain at a creep stage changes according to the location after the reversal point (point c_2). Therefore, we may assume that a neutral point exists and corresponds to a creep stage, which is characterized by strain amplitude vanishing to zero. This phenomenon is brought to the fore by creeps d_2e_2 and i_2j_2 in figure 3. Hence, the neutral points are located on the unloading branch between creeps d_2e_2 and f_2g_2, and on the reloading branch between relaxations i_2j_2 and k_2l_2 [2].

Figure 5 compares the results of a test 1 and the beginning of test 2. In this figure the starts and ends of the creep sequences are shown by black squares and black triangles, respectively. In order to characterize the evolutions of the starts and ends of creep sequences, we adopted a simple model, such as:

$$\sigma_m(\varepsilon_l) = S_0\ \mathrm{th}\left(\frac{M_0}{S_0}\,\varepsilon_l\right) \qquad \textbf{(5)}$$

where S_0 denotes a parameter associated with a stress threshold and M_0 an elastic modulus in the stress-strain diagram, such as:

$$M_0 = \lim_{\varepsilon_l \to 0} \frac{d\sigma_m}{d\varepsilon_l}(\varepsilon_l)$$

Figure 5 gives the curves of starts and ends of creep sequences, identified with the previous model (eq. 5).

The parameter values obtained are:

M_0=2.6 kJ/g and S_0=52 J/g for the curve 'start of creep periods' and M_0=2.0 kJ/g and S_0= 46 J/g for the curve 'end of creep periods' (Fig.5).

We note a difference in elastic modulus, between these two curves, of 30%. This result, obtained for $\dot{\sigma}_m = 671\ J/(kg.s)$, depends strongly on the stress rate. This result underlines the importance of viscous effects, which may have a significant impact on the structural behaviour of sails, even in small deformation.

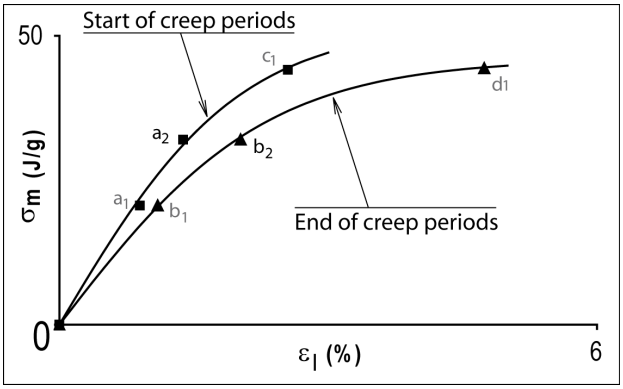

Figure 5 - Change in behaviour between start and end of the creep periods ($\dot{\sigma}_m = 671\ J/(kg.s)$)

4.2 MONOTONOUS TENSILE TESTS AT CONSTANT STRAIN RATE

Monotonous tensile tests at constant strain rates were performed with "Dacron 300 SF HTM", in warp and fill directions. During these tests, the strain rate was maintained constant at D=$10^{-3}s^{-1}$. Figure 6 presents some typical results in the stress-strain diagram. Some tests were broken with a stress relaxation period at a constant strain (relaxation ab), and other ended by a stress relaxation period (relaxation cd). The curves are composed of three zones; in the first zone the stress is less than 30 J/g, the second zone is between about 40 and 80 J/g and the third zone presents stresses above 80 J/g. The transition between the first and the second zone is sharp and the transition between the second and third zone is very gradual. During the reloading just after the relaxation period ab, the slope in the stress–strain graph is one of the highest. Moreover, the transient state just after a relaxation period ab presents a particular shape, like an overshoot above the steady state stress; firstly the stress rises linearly with the strain and soon beyond the steady state stress and then

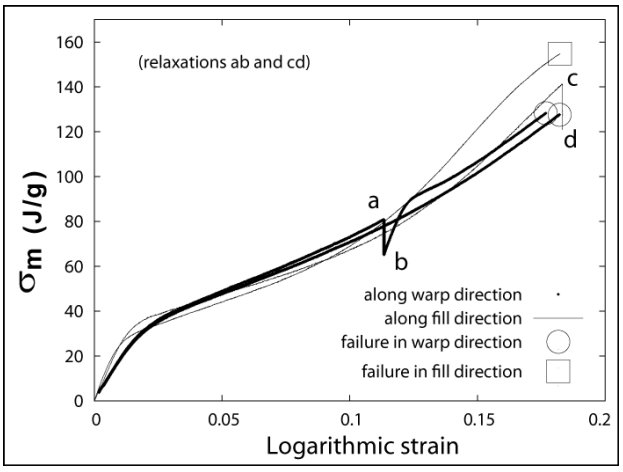

Figure 6: Results of monotonous tensile tests

decreases in a second step and reaches this steady state stress.

The results of these tests were used to characterize mechanical parameters, as following:

- In the warp direction

Young modulus = 1727 ± 28 J/g (68% c.i., n = 5)
Poisson's ratio = $0{,}020 \pm 0{,}004$ (68% c.i., n = 5)
Failure stress = 122 ± 11 J/g (68% c.i., n = 5)
Failure strain = $0{,}174 \pm 0{,}015$ (68% c.i., n = 5)

- In the fill direction

Young modulus = 2850 ± 130 J/g (68% c.i., n = 5)
Poisson's ratio = $0{,}046 \pm 0{,}005$ (68% c.i., n = 5)
Failure stress = 147 ± 12 J/g (68% c.i., n = 5)
Failure strain = $0{,}177 \pm 0{,}020$ (68% c.i., n = 5)

The above results and the figure show that the warp and fill directions was distinguished basically by their elastic modulus and by their failure stress. Sun et al. [12] present Poisson's ratios of polyester fabrics of 0.20 and 0.34. The difference between these values and our measures should be due to the fact that they consider the Poisson's ratio at very small strains.

4.3 CREEP AND RELAXATION BEHAVIOUR

Figure 7 groups the creep curves obtained during test 2 (Fig. 3). The axes of figure 7 are such as:

$$\Delta t = t - t_0 \ , \ \Delta\varepsilon_l(t) = \left|\varepsilon_l - \varepsilon_l^{\,0}\right| \quad \textbf{(6)}$$

and t_0, $\varepsilon_l^{\,0}$ correspond to the time and the logarithmic strain at the beginning of the creep stages. The time evolution of the creep strain presents a typical shape of most creeps whatever their location in the loading [6, 8]. The time evolution of the strain, during a creep stage predicted by the classic linear viscoelastic Maxwell model, is also presented in figure 7 (curve a). This evolution is of an exponential type. The two parameters of the Maxwell model were calculated in order to take into account the whole variation of strain

during the creep and the strain rate at the beginning of the creep period. Figure 7 underscores a fundamental difference of strain curve shapes between the linear viscoelastic Maxwell model and test 2. The time evolution of Maxwell strain reaches its limit in a duration equal to about three times its characteristic time θ. Whereas the time evolutions of the strain during test 2 increase more and more slowly and do not show any threshold or asymptotic limit. These experimental time evolutions during creep stages show a typical shape that could be defined by a theoretical equation as follows:

$$\frac{\Delta\varepsilon_l}{\Delta\varepsilon_l^{Max}} = A\ Log(\Delta t) + B \qquad (7)$$

where A = 0,23, B = 0.18 for curve (b) and A = 0,46, B =-0.67 for curve (c). Figure 7 allows us to compare the experimental results with the two curves corresponding to the basic relaxation model defined by relation 7; there is a good accordance between them. Indeed, the curves (b) and (c) define a high and low limit which include all results.

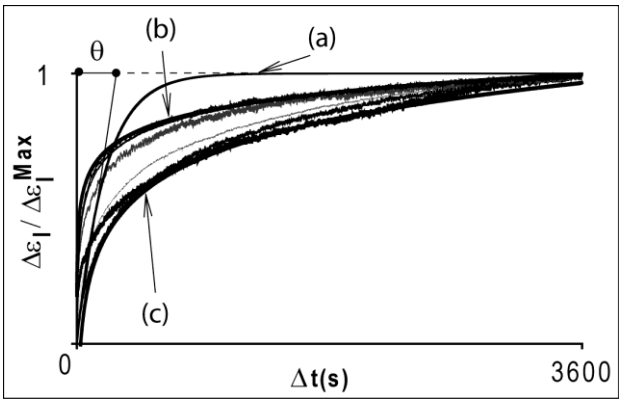

Figure 7: Comparison of the time evolutions of creep strain of test 2 (Fig. 3) to the linear viscoelastic Maxwell model prediction (curve a) and to creep behaviour according to relation 7 (curve b and c)

In the same way, figure 8 gives the time evolution of stress relaxations ab and cd of figure 6. This figure suggests qualitatively that the type of time evolution of stress relaxation is similar to that of creep strain defined by relation 7 [2].

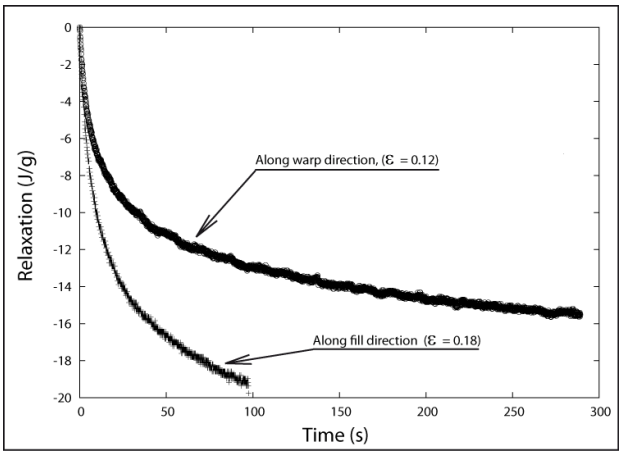

Figure 8: Time evolution of stress relaxations ab and cd of figure 6.

5. IMPLEMENTATION OF THE PROPOSED APPROACH IN THE LINEAR VISCOELASTIC CASE

To reduce the analysis to essentials and focus attention on the influence of viscous behaviour, we consider the linear viscoelastic case. Considering this simplifying assumption the relation (1) is reduced to:

$$\sigma(\varepsilon,\dot{\varepsilon}) = \sigma_v(\dot{\varepsilon}) + \sigma_r(\varepsilon)$$

And in the isotropic biaxial case the constitutive law is defined by the following relations:

$$\overline{\overline{\sigma}} = \overline{\overline{\sigma_v}} + \overline{\overline{\sigma_r}}$$

$$\overline{\overline{\sigma_r}} = \lambda_r . Tr(\overline{\overline{LnV}}).\overline{\overline{I}} + 2\mu_r . \overline{\overline{LnV}}$$

$$\overset{\circ rp}{\overline{\overline{\sigma_v}}} + \frac{\overline{\overline{\sigma_v}}}{\theta_v} = \lambda_v . Tr(\overline{\overline{D}}).\overline{\overline{I}} + 2\mu_v . \overline{\overline{D}}$$

$\overline{\overline{LnV}}$ is the logarithmic eulerian strain. The time derivative $\overset{\circ rp}{\overline{\overline{A}}}$ of a second-order tensor $\overline{\overline{A}}$ is the Green-Naghdi objective rate.

The constitutive law is implemented in membrane-like case, such as:

$$\lambda_a = \frac{E_a.\nu_a}{(1+\nu_a)(1-\nu_a)} \quad \mu_a = \frac{E_a.\nu_a}{2(1+\nu_a)} \qquad (8)$$

The sign ‘a’ is equal to r in the reversible case and equal to v in the viscous case. Let us note that, in membrane-like case, some classic equations are transformed, like for example the classic relations between the elastic parameters of Hooke law (eq.8) or the trace operator of identity tensor:

$$Tr\overline{\overline{I}} = 2$$

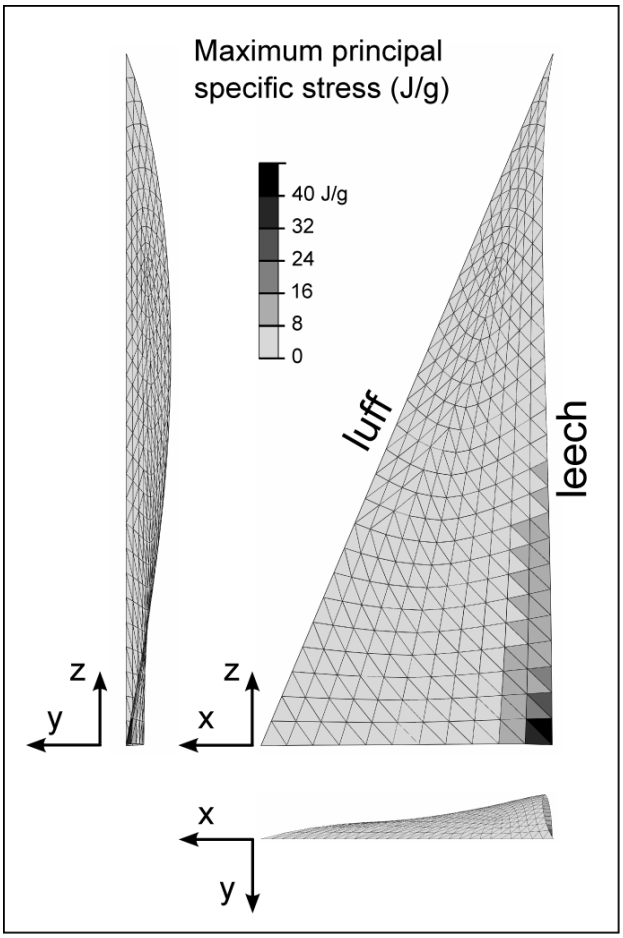

Figure 9: Meshed flat sail geometry and maximum principal specific stress

The mechanical behaviour of a flat sail has been simulated by the commercial finite element code ABAQUS. The whole sail is made with "Dacron 300 SF HTM", which is supposed isotropic material. The model parameters were identified using the tensile tests along the warp direction:

- Young modulus of viscous stress = 1413 J/g
- Poisson's ratio of viscous stress = 0.02
- Relaxation time of viscous stress = 11 s
- Young modulus of elastic stress = 570 J/g
- Poisson's ratio of elastic stress = 0.02

Fully integrated solid elements (M3D3; 544 linear membrane elements, 3-node triangle) were used, as presented in Fig. 9. The nodes of the luff and the clew node are pinned, i.e. their displacements are null. A homogeneous pressure is applied on the sail. Nonlinearities due to large deflections are taken into account (*Nlgeom* option of code Abaqus). For instance, the pressure load follows the rotation of the elements. The strain definition does not assume small displacements.

To evaluate the sail stiffness and characterize the viscous effect, the leech position is plotted in the y (horizontal) and z (vertical) plane (Fig. 10). The first phase of loading corresponds to a constant pressure P=80 Pa. The second phase of the load P=150Pa is then applied. The span of rising in pressure between the first and second phase is 2 seconds. Pressure P=150Pa is maintained constant during 2 minutes in the last phase of loading.

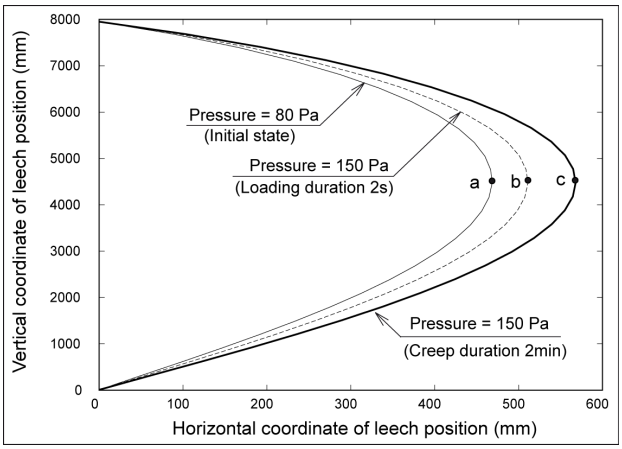

Figure 10: Deformation of the sail during loading

The tip displacement (points a, b and c) between b and c corresponds about 30% higher than the tip displacement between a and b. This result is a consequence of results already archived in section 4.1. The viscous behaviour of material may have a significant impact on the structural behaviour of sails, even in small deformation. Indeed, the pressure applied to the sail correspond to a quite reasonable wind speeds, about 22kn for P=80Pa and 30 kn for P = 150Pa.

6. CONCLUSIONS

Monotonous and cyclic tensile loadings with creep and relaxation periods were carried out at constant strain and stress rates. The experimental study is completed by an implementation of the proposed theoretical approach in the linear viscoelastic case. A structural analysis of a flat sail is proposed using finite element method. The results underline the importance of viscous effects, which may have a significant impact on the structural behaviour of sails, even in small deformation.

7. REFERENCES

1. BLES, G., GADAJ, S.P., GUELIN, P., NOWACKI, W.K., TOURABI, A., 'Thermomechanics of viscoplastic large strains of solid polymers', *Archives of Mechanics 52 (3), p.397–427*, 2000.

2. BLES, G., NOWACKI, W.K., TOURABI, A., 'Experimental study of the cyclic visco-elasto-plastic behaviour of a polyamide fibre strap', *International Journal of Solids and Structures 46, p.2693–2705*, 2009.

3. BLES, G., GADAJ, NOWACKI, W.K., TOURABI, A., 'Experimental study of a PA66 solid polymer in the case of shear cyclic loading.', *Archives of Mechanics 54 (2), p.155–174*, 2002.

4. BLES, G., NOWACKI, W.K., TOURABI, A., 'Viscoelastoplastic thermomechanical constitutive patterns at high rates of strain', *Journal of Physics 10 (Pr9), p.27–32*, 2000.

5. BOISSE, P., GASSER, A., HIVET, G., 'Analyses of fabric tensile behaviour: determination of the biaxial tension±strain surfaces and their use in forming simulations ', *Composites: Part A 32, p.1395-1414*, 2001.

6. DROZDOV, A.D., CHRISTIANSEN, J.DEC., 'Constitutive equations for the nonlinear viscoelastic and viscoplastic behaviour of thermoplastic elastomers', *International Journal of Engineering Science 44, p.205-226*, 2006,

7. LE MAITRE, O., SOUZA DE CURSI, J.E., HUBERSON, S., 'Large displacement analysis for ideally flexible sails', *Eur. J. Mech. A/Solids 17 (4), p.619-636*, 1998.

8. MIEHE, C., GÖKTEPE, S., 'A micro-macro approach to rubber-like materials - Part II: The micro-sphere model of finite rubber viscoelasticity', *Journal of the Mechanics and Physics of Solids 53, p.2231-2258*, 2005.

9. PAROLINI, N., QUARTERONI, A., 'Mathematical models and numerical simulations for the America's Cup', *Comput. Methods Appl. Mech. Engrg. 194, p.1001-1026*, 2005.

10. PATON, J., MORVAN, H.P., HEPPEL, P. 'Fluid structure interaction of yacht sails', *Innov'Sail2008 International Conference on Innovation in High Performance Sailing Yachts (The Royal Institution of Naval Architects), Lorient, France*, 2008.

11. SPALATELU-LAZAR, M., LENE, F., TURBE, N. 'Modelling and optimization of sails', *Computers and Structures 86, p.1486-1493*, 2008.

12. SUN, H., PAN, N., POSTLE, R. 'On the Poisson's ratios of a woven fabric', *Composite Structures 68, p.505-510*, 2005.

13. TOURABI, A., GUELIN, P., FAVIER, D., 'Towards modelling of deformable ferromagnets and ferroelectrics', *Archives of Mechanics 47 (3), p.294–323*, 1995.

14. TOURABI, A., GUELIN, P., FAVIER, D., NOWACKI, W.K., 'From material discrete memory patterns to the study of demagnetization-like processes', *Archives of Mechanics 49 (4), p.737–766*, 1997.

15. VALDES, J.G., MIQUEL, J., ONATE, E. 'Nonlinear finite element analysis of orthotropic and prestressed membrane structures', *Finite Elements in Analysis and Design 45, p.395-405*, 2009.

8. AUTHORS BIOGRAPHY

Wassim Dib PhD student at University of Grenoble and Engineering School ENSIETA of Brest (France).
Guilhem Bles Doctor's degree in Solid Mechanics, Senior Lecturer at ENSIETA – BREST (France).
Ali Tourabi Doctor's degree in Solid Mechanics, Senior Lecturer at Joseph Fourier University – Grenoble (France).